

EXPLORING THE IMPACT OF A THREE-BODY INTERACTION ADDED TO THE GRAVITATIONAL POTENTIAL FUNCTION IN THE RESTRICTED THREE-BODY PROBLEM

Natasha Bosanac*, Kathleen C. Howell[†], and Ephraim Fischbach[‡]

Many binary star systems (e.g., pulsar-white dwarf) are known to possess significantly smaller companions, such as an exoplanet, in orbit about the binary. In this investigation, the dynamical environment near the binary is modeled using a three-body interaction added to the inverse-square pairwise gravitational forces in the circular, restricted three-body problem (CR3BP), given a mass ratio of 0.3. This additional force contribution is assumed to depend inversely on the product of the distances between the three bodies. Frequency analysis is used to characterize the effect of this three-body interaction on periodic and quasi-periodic orbits in the exterior region for a large mass ratio binary. Sufficiently scaled attractive three-body interactions appear to induce period-multiplying bifurcations, with a low multiplicative factor, along families of periodic orbits, an effect that is not reproducible using large mass ratios in the range $[0.2, 0.4]$ in the CR3BP. Repulsive three-body interactions appear to impact the formation of families of periodic orbits, influencing the location of stable and unstable orbits within a periodic orbit island chain. In addition, repulsive interactions influence the openings of the Lagrange point gateways, as compared with the CR3BP.

INTRODUCTION

Consider a binary star system (e.g., pulsar-white dwarf, pulsar-pulsar) with a significantly smaller companion, such as an exoplanet, in orbit about the binary. Such a dynamical scenario has been both speculated and observed by astronomers in a variety of star systems far beyond the boundaries of the solar system.¹ However, given the absence of experimental data gathered within the vicinity of the binary, it is possible that the gravitational field within this system might not be accurately modeled solely using pairwise gravitational forces. In this investigation, the presence of an additional three-body interaction is considered. Many-body forces are not an entirely new concept; in fact, the importance of three-body interactions in accurately modeling force fields on the atomic scale is well established in nuclear physics.² On a much larger scale, the motion of a small body orbiting a binary star system serves as a new and interesting application for determining the characteristics of a three-body interaction in orbital dynamics.

Since binary star systems are located many light-years from the Earth, the characteristics of the binary, and any smaller companions, are determined from pulsar timing measurements;³ the availability of timing data renders such binaries suitable applications for exploring the influence of a three-body interaction. A pulsar in complete isolation would rotate about its spin axis with a constant angular velocity, emitting pulses of radiation at a constant rate. However, in the presence of additional bodies, the pulsar appears to rotate with a nonconstant angular velocity. The resulting Doppler shift in the timing of the pulses is approximately fitted to the orbit of the pulsar, which is typically correlated to the masses and orbits of any companions. These orbits are governed by a dynamical environment that may be modeled using various interactions, including those due to pairwise point-mass gravity, gravitational wave radiation, and magnetic fields.

*Graduate Student, School of Aeronautics and Astronautics, Purdue University, 701 W. Stadium Ave., West Lafayette, Indiana 47907-2045.

[†]Hsu Lo Professor of Aeronautical and Astronautical Engineering, School of Aeronautics and Astronautics, Purdue University, 701 W. Stadium Ave., West Lafayette, Indiana 47907-2045.

[‡]Professor of Physics, Department of Physics, Purdue University, 525 Northwestern Ave., West Lafayette, Indiana 47907-2045.

The dynamical model for the motion of the exoplanet is derived based on the circular restricted three-body problem (CR3BP), but extended to incorporate an additional term in the potential function: a three-body interaction. This additional contribution is assumed to depend inversely on the product of the distances between the three bodies: the closer the bodies, the stronger the three-body interaction. The subsequent set of differential equations comprises the framework for a modified circular restricted three-body problem (MCR3BP). In the configuration modeled in this investigation, the two stars comprising the binary are assumed to possess similar mass and follow circular paths about their mutual barycenter. Although a large mass ratio reflects the physical configuration of many binary star systems, it is significantly larger than the mass ratios of natural systems considered within the solar system.

This investigation is comprised of two parts. First, the characteristics of the CR3BP are explored for a relatively large mass ratio. Natural solutions in the MCR3BP are then analyzed and compared to those in the CR3BP to explore the effect of the three-body interaction. Given that many of the known binary star systems are postulated to possess one or more exoplanets in large orbits about both stars, this investigation of three-body interactions is currently limited to the study of trajectories far from the binary. For an exoplanet to be bound to the vicinity of the binary over a long period of time, it likely exhibits ordered motion that is not sensitive to perturbations. These orbits can be decomposed into the sum of multiple sinusoidal waves that are characterized by their fundamental frequencies. Monitoring the influence of a three-body interaction on any fundamental frequencies may represent the potential impact on the behavior of an exoplanet. Thus, frequency analysis is employed to investigate the effect of the additional three-body contribution on the dynamical environment in the vicinity of a binary.

DYNAMICAL MODEL

The MCR3BP is formulated similar to the traditional CR3BP.⁴ Although the notation and the general configuration are consistent between the two systems, the MCR3BP incorporates the presence of three-body interactions in addition to pairwise gravitational interactions. The form of the augmented potential in the MCR3BP influences the equations of motion, yielding a model that still admits an integral of the motion. Particular solutions, in the form of equilibrium points and zero velocity curves, are also available in this augmented model and still establish bounds on the motion.⁴

Rotating Coordinate Frame and Nondimensionalization

By convention, the body of interest, P_3 , moves in the vicinity of the larger and smaller primaries, P_1 and P_2 , each body P_i possessing a mass M_i . Figure 1 depicts the configuration of these three bodies. As in the CR3BP, a rotating coordinate frame, $\hat{x}\hat{y}\hat{z}$, is introduced and oriented relative to an inertial frame, $\hat{X}\hat{Y}\hat{Z}$. In the frame that rotates with the motion of the two primaries the location of P_3 , measured with respect to the barycenter, is written in terms of the nondimensional coordinates (x, y, z) . Consistent with the CR3BP, length quantities are nondimensionalized such that the distance between P_1 and P_2 is equal to a constant value of 1. In addition, time is nondimensionalized such that the mean motion of the primaries is equal to 1, while the characteristic mass quantity, m^* , is the sum of the masses of the primaries. The characteristic mass quantity yields nondimensional mass values for P_2 and P_1 equal to μ and $(1 - \mu)$, respectively. In the first half of this investigation, the mass ratio is varied within the range $\mu = [0.2, 0.4]$. During analysis of the MCR3BP, however, the value for μ is fixed at 0.30. This large mass ratio has not been explored extensively from the perspective of the CR3BP. It is, however, representative of the order of magnitude corresponding to many binary pulsar systems, such as the pulsar-white dwarf binary system PSR B1620-26 that is known to include at least one exoplanet.³

Equations of Motion

Given a system configuration consistent with the CR3BP, derivation of the differential equations governing the motion of P_3 in the MCR3BP requires the definition of the potential function. In the rotating frame, the

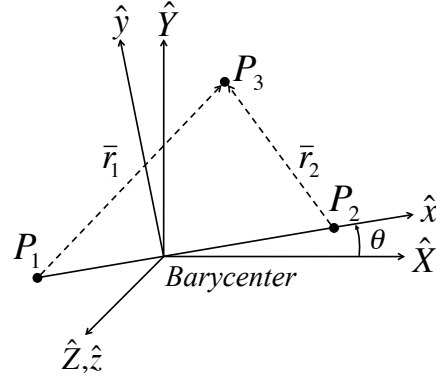


Figure 1. Definition of the rotating coordinate frame with a constant angular velocity relative to the inertial frame at a nondimensional rate of unity about the \hat{Z} -axis.

scalar potential corresponding to P_3 , per unit mass, is assumed to consist of the following terms:

$$U_3 = \underbrace{\frac{1-\mu}{r_1} + \frac{\mu}{r_2}}_{\text{pairwise potential}} + \underbrace{\frac{k}{r_1 r_2}}_{\text{three-body potential}} \quad (1)$$

where $r_1 = \sqrt{(x+\mu)^2 + y^2 + z^2}$ and $r_2 = \sqrt{(x-1+\mu)^2 + y^2 + z^2}$ are the nondimensional distances between P_3 and each of the primaries, and k is the constant that scales the contribution of the three-body interaction to the resultant potential. Since the magnitude and sign of this constant are unknown, it is assumed that k can be selected as either positive, negative or zero. When the value of the constant k is equal to zero, the potential of the MCR3BP reduces to the CR3BP potential; if k is positive, the three-body interaction is attractive, while a negative value of the coefficient corresponds to a repulsive interaction.

From the definition of the potential function in Equation (1), the equations of motion for P_3 are derived and a constant of motion is subsequently identified. Since the potential function depends only upon position variables, it is differentiated to determine the force per unit mass acting on the body, P_3 . The equations of motion in terms of the rotating frame are then written as:

$$\ddot{x} = 2\dot{y} + x - \frac{(1-\mu)(x+\mu)}{r_1^3} - \frac{\mu(x-1+\mu)}{r_2^3} - k \left[\frac{(x-1+\mu)}{r_1 r_2^3} + \frac{(x+\mu)}{r_1^3 r_2} \right] \quad (2)$$

$$\ddot{y} = -2\dot{x} + y - \frac{(1-\mu)y}{r_1^3} - \frac{\mu y}{r_2^3} - k \left[\frac{y}{r_1 r_2^3} + \frac{y}{r_1^3 r_2} \right] \quad (3)$$

$$\ddot{z} = -\frac{(1-\mu)z}{r_1^3} - \frac{\mu z}{r_2^3} - k \left[\frac{z}{r_1 r_2^3} + \frac{z}{r_1^3 r_2} \right] \quad (4)$$

Although the complete, three-dimensional equations of motion are available, only planar solutions are considered throughout this investigation. The equations of motion can then be written in terms of the partial derivatives of U^* , the pseudopotential function.⁴ This quantity is exploited to develop the energy integral that corresponds to the equations of motion as formulated in the rotating frame. Since the pseudopotential is autonomous, its derivative with respect to time is always equal to zero. A constant energy integral, C , therefore, exists and is equal to:

$$C = x^2 + y^2 + \frac{2(1-\mu)}{r_1} + \frac{2\mu}{r_2} + \frac{2k}{r_1 r_2} - \dot{x}^2 - \dot{y}^2 - \dot{z}^2 \quad (5)$$

When the contribution of the three-body potential is omitted by selecting $k = 0$, this energy integral reduces to the well-known Jacobi Constant of the CR3BP.⁵ Given that there are infinite possible sets of initial conditions

in the form of six position and relative velocity states, $(x, y, z, \dot{x}, \dot{y}, \dot{z})$, numerical methods and visualization techniques are employed to explore the solution space. At various values of the energy constant, a wide array of behavior may exist, and the corresponding steady-state solutions are characterized using concepts developed in dynamical systems theory.

TIME-VARYING SOLUTIONS

Since the equations of motion in the CR3BP are nonintegrable and autonomous, four types of steady-state solutions exist: equilibrium points, periodic orbits, quasi-periodic orbits, and chaotic motion.⁶ Each of these solutions, for a mass ratio of $\mu = 0.3$, is plotted in Figure 2(a)-(d) in position space, with blue filled circles indicating the location of the primaries. While the equilibrium point locations remain constant over time, periodic solutions are time-varying and repeatable. In the rotating coordinate system, a period- q orbit can encircle the primaries or an equilibrium point q times during one period, T . The dense set of periodic orbits in the CR3BP forms the underlying structure of the phase space: a stable orbit attracts trajectories in its vicinity, while trajectories near an unstable orbit flow away from the orbit.⁷ Thus, identifying periodic orbits and evaluating their stability delivers significant insight into the behavior in their vicinity. Quasi-periodic orbits offer additional information concerning the dynamical environment. Such orbits are bounded and each traces out a torus, with a nearby stable periodic orbit at its center.⁵ Investigating the properties of quasi-periodic orbits and their excursions within the phase space enables a representation of the significant stable dynamics within the CR3BP.

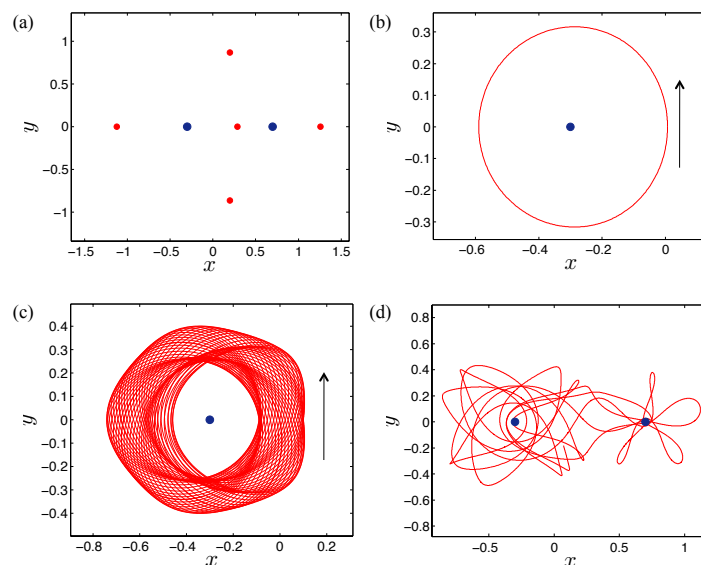


Figure 2. Examples of steady-state solutions in the CR3BP for $\mu = 0.3$: (a) equilibrium points, (b) a periodic orbit, (c) a quasi-periodic orbit, and (d) chaotic motion.

Stability

The stability of a periodic orbit is typically deduced from the monodromy matrix, defined as the state transition matrix (STM) propagated for precisely one period of the orbit.⁸ Given a reference planar periodic orbit, the solution that approximates a nearby arc is determined using the linear variational equations of motion. The solution describing the relative neighboring arc is written as:

$$\delta\bar{x}(t) = \Phi(t, 0)\delta\bar{x}(t_0)$$

where $\delta\bar{x}(t_0)$ is the vector variation with respect to the initial state along the orbit and $\Phi(t, 0)$ is the state transition matrix, essentially a linear mapping from t_0 to a time t .⁹ Via Floquet theory, the monodromy

matrix of the reference periodic orbit is decomposed into the following form:

$$\Phi(T, 0) = \mathbf{V}(0)e^{\Omega T}\mathbf{V}(0)^{-1} \quad (6)$$

where the diagonal elements of Ω are the Poincaré exponents, Ω_i , for $i = 1 \dots 4$.⁹ Since $e^{\Omega T}$ is a diagonal matrix, $\mathbf{V}(0)$ is a matrix that is formed from the eigenvectors of the monodromy matrix, $\Phi(T, 0)$, and the Poincaré exponents are related to its eigenvalues such that $\lambda_i = e^{\Omega_i T}$. The eigenvalues of the monodromy matrix reflect the characteristics of the underlying linear system; however, the nontrivial eigenvalues also supply insight into the stability of the periodic orbit in the original, nonlinear system. Each planar, periodic orbit possesses a monodromy matrix that can be decomposed into four eigenvalues and their associated eigenvectors.⁹ Two of the eigenvalues are equal to unity due to periodicity; the other two nontrivial eigenvalues may be represented in the form $\lambda = a \pm bi$, in terms of two real numbers, a and b . Depending on the value of these integers, three specific cases of eigenvalues emerge: real, complex, and imaginary. Regardless of the form of these eigenvalues, they appear as a reciprocal pair due to the symplectic properties of the state transition matrix. From the Lyapunov definition of stability, stable periodic orbits possess a nontrivial pair of complex or imaginary eigenvalues, $\lambda_1, \lambda_2 = a \pm bi$. A pair of reciprocal eigenvalues, $|\lambda_1| = a > 1$ and $|\lambda_2| = 1/a < 1$, however, correspond to an unstable periodic orbit.⁸ Since the stability of an orbit reflects the behavior of solutions within its vicinity, a monodromy matrix that possesses complex eigenvalues indicates the oscillatory motion of nearby quasi-periodic orbits.

Bifurcations

In the CR3BP, periodic orbits exist in families that, for a given mass ratio, depend upon the energy constant. Varying C , the natural parameter, directly modifies the vector field, $\dot{f}(\bar{x})$, and, therefore, its infinite set of solutions. A local bifurcation occurs if a change in the energy constant results in a change in the qualitative behavior of trajectories in the vicinity of a periodic orbit. In dynamical systems, a bifurcation may result in a change in the stability of the periodic orbits along a family, the formation of a new family of periodic orbits, or termination of the current family.¹⁰ Since the stability of a periodic orbit reflects the behavior of nearby trajectories, local bifurcations are detected and characterized by monitoring the pair of nontrivial eigenvalues of the monodromy matrix corresponding to each periodic orbit along a family. Introducing an alternative representation of the nontrivial eigenvalues, a stability index is employed. This quantity is defined as the sum of the two reciprocal eigenvalues, equal to $s = \lambda + \frac{1}{\lambda}$. Given the form of this expression, possible bifurcations can be detected through changes in the stability of the periodic orbits comprising a family, reflected by the stability index passing through any critical values.

Although many possible bifurcations exist, two types emerge within the dynamical environment that is the focus of this investigation: tangent and period-multiplying bifurcations. A family of periodic orbits undergoes a tangent bifurcation when the qualitative stability characteristics of its orbits change with the energy constant. During this type of local bifurcation, the nontrivial eigenvalues of the monodromy matrix pass through the critical values $\lambda_1 = \lambda_2 = +1$. Simultaneously, the stability index passes through $s = 2$. Depending on the type of tangent bifurcation, the change in stability may be accompanied by the creation of families of similar period or by the intersection with another family of orbits. Across each form of tangent bifurcation, the eigenvalues that reflect the stability of the orbits along a family transition between the unit circle and the real axis. During a period-multiplying bifurcation of multiplicative factor m , a family of period- m orbits emerges from a family of period- q orbits. At the critical value of the natural parameter, the orbit located at the intersection of the two families is equivalently described as a period- m orbit or a period- q orbit traced out m times. Employing properties of the STM, this bifurcation is detected when the eigenvalues of the period- q orbits along a family pass through the first and $(m - 1)$ -th complex roots of unity, that are equal to:

$$\lambda_1, \lambda_2 = \cos\left(\frac{2\pi}{m}\right) \pm \sin\left(\frac{2\pi}{m}\right) i \quad (7)$$

or, equivalently, when the stability index passes through the critical value:

$$s = 2 \cos\left(\frac{2\pi}{m}\right) \quad (8)$$

Since the stability index does not reflect the imaginary components of any complex conjugate eigenvalues, confirmation of a period-multiplying bifurcation requires verification that the eigenvalues do not split off the unit circle after passing through the corresponding roots of unity.

Quasi-Periodic Orbits

Stable periodic orbits are typically surrounded by quasi-periodic orbits, corresponding to nonperiodic, bounded motion that lies on a two-dimensional torus.⁷ A torus is parameterized using two noncommensurate, fundamental frequencies:⁵ the central frequency, ω_1 , in the direction of the periodic orbit, and ω_2 , the transverse frequency. A quasi-periodic orbit is reconstructed using sinusoidal waves with frequencies that are equal to linear combinations of these two fundamental frequencies. When the two dominant frequencies are commensurate, their ratio is equated to the ratio of two integers: a limiting case that corresponds to a resonant periodic orbit. Computing and interpreting the frequency decomposition of ordered motion is, therefore, a key element in the analysis of the dynamics in the CR3BP.

FREQUENCY ANALYSIS

Frequency analysis can be used to characterize a quasi-periodic orbit by decomposing its trajectory into linear combinations of the fundamental frequencies of the oscillatory motion in each of the central and transverse directions. A variable, $y(t)$, corresponding to a quasi-periodic orbit, can be expressed using a Fourier series in rectangular form as:

$$y(t) = \sum_{m=1}^{\infty} (A_m \cos(2\pi(r_m\omega_1 + s_m\omega_2)t) + B_m \sin(2\pi(r_m\omega_1 + s_m\omega_2)t)) \quad (9)$$

where A_m and B_m are, respectively, the coefficients of the cosine and sine components for the m -th dominant linear combination of the fundamental frequencies, $\omega_m = (r_m\omega_1 + s_m\omega_2)$, for the integers r_m and s_m . Various properties of quasi-periodic orbits are identifiable from the fundamental frequencies and some significant characteristics can be deduced. These frequencies can directly represent: (i) the presence of resonant orbits, (ii) a qualitative evaluation of the orbital stability, (iii) an estimate of the orbital period (to within an integer ratio) and, (iv) through either the number of map crossings of a periodic orbit or the number of stable islands on a map, the existence of a quasi-periodic orbit (to within an integer ratio). Frequency analysis is, therefore, an appropriate basis from which to explore the influence of three-body interactions on the form and prevalence of ordered motion in the MCR3BP.

The numerical approach to frequency analysis, which is adopted in this investigation, is based on Laskar's Numerical Analysis of the Fundamental Frequency (NAFF algorithm).¹¹ Laskar's method decomposes a trajectory, integrated over a finite time interval, into a finite set of sinusoidal waves. A differential corrections algorithm is employed to iteratively update the initial guess for each sinusoidal wave until the trajectory is sufficiently reconstructed from the dominant linear combinations of the two fundamental frequencies. From an implementation perspective, the NAFF algorithm requires less memory and computational time than the construction of a normal form for the dynamical topology in the vicinity of a periodic orbit. Thus, Laskar's method is employed in this initial investigation.

Discrete Fourier Transform

Each of the numerically integrated trajectories in this investigation are actually only composed of a set of states at a finite set of times, yielding discrete time-dependent functions. A Discrete Fourier Transform (DFT) is, therefore, employed to determine the underlying frequencies of each numerically integrated path and the coefficients describing the corresponding sinusoidal wave. Assume that a continuous function, $y(t)$, is sampled at N equally-spaced time intervals, each of length Δt , where N is assumed to be even. Each point along the function, sampled at $t_n = n\Delta t$, possesses a value $\tilde{y}(n)$ corresponding to the integer time indices $n = 0, 1, \dots, N - 1$. The N samples, $\tilde{y}(n)$, in the time domain, are then transformed into the N values of

$\tilde{Y}(m)$ in the frequency domain using the DFT, defined as:

$$\tilde{Y}(m) = \sum_{n=0}^{N-1} \tilde{y}(n) (\cos(2\pi mn/N) - i \sin(2\pi mn/N)) \quad (10)$$

for the m -th frequency, $\omega_m = \frac{m}{N\Delta t}$. The rectangular coefficients for each sinusoidal wave, with frequency ω_m , are subsequently computed as:

$$\tilde{A}_m = \frac{1}{N} \sum_{n=0}^{N-1} \tilde{y}(n) \cos(2\pi mn/N) \quad \tilde{B}_m = \frac{-1}{N} \sum_{n=0}^{N-1} \tilde{y}(n) \sin(2\pi mn/N) \quad (11)$$

where the tilde indicates that the original function is discrete in the time domain. Given knowledge of a finite number of these sinusoidal wave coefficients and their corresponding frequencies, the original function is reconstructed using a truncated Fourier series expansion.

Numerical Frequency-Refinement

The limitations of the DFT are apparent when a frequency decomposition is applied to numerically integrated trajectories in the CR3BP. Although the accuracy of the resulting frequency decomposition theoretically improves as the integration time increases, small errors in the analyzed function accumulate over long integration times. The integration time interval is, therefore, selected to supply sufficient resolution in the frequency spectrum, while maintaining an accurate representation of a natural trajectory in the CR3BP. For the implementation in this analysis, constraints on the computation time, as well as the allowable variation of the energy constant, limit the maximum integration time to a range between 5,000 and 10,000 nondimensional time units: corresponding to approximately 500-1000 revolutions about the primaries. For a trajectory propagated over this time span, the accuracy of any frequency computed via the DFT, using a Hanning window, is on the order of 10^{-4} (nondimensional time units) $^{-1}$. In the CR3BP, the fundamental frequencies corresponding to the quasi-periodic orbits within a stable island at a given energy level can vary by a smaller order of magnitude than the accuracy obtained through the use of a DFT, implemented using an FFT algorithm. Thus, a frequency resolution of 10^{-4} is considered insufficient for this application. A targeting scheme is, therefore, implemented to individually refine the parameters that describe the trajectory of interest.

The differential corrections scheme implemented in this investigation is formulated such that free variables are iteratively updated to satisfy a defined set of constraints. In particular, the independent elements of the free-variable vector available for adjustment correspond to the parameters describing the j -th sinusoidal wave. Three real-valued parameters, therefore, form the free variable vector, \bar{X} :

$$\bar{X} = [\omega_j \quad A_j \quad B_j]^T \quad (12)$$

The sinusoidal wave constructed from the initial guess for the free variable vector is iteratively refined until it coincides with one of the sinusoidal waves comprising the original function, $\tilde{y}(t_n)$. Constraints can, therefore, be formulated to target the local maximum amplitude of the following quantity:

$$u(\omega_j) = \frac{1}{N} \sum_{n=1}^N \tilde{y}(t_n) [\cos(2\pi\omega_j t_n) - \sin(2\pi\omega_j t_n)i] \quad (13)$$

where N is the number of points comprising the discrete function $\tilde{y}(t_n)$. Differentiating $u(\omega_j)$, and writing the result in terms of the independent set of free variables, produces the frequency constraint:

$$\frac{\partial u(\omega_j)}{\partial \omega_j} = \frac{2}{\sqrt{D_c^2 + D_s^2}} \left[D_c \frac{\partial D_c}{\partial \omega_j} + D_s \frac{\partial D_s}{\partial \omega_j} \right] = 0 \quad (14)$$

where D_c and D_s are, respectively, the real and imaginary components of the rectangular form of $u(\omega_j)$. These two variables are computed as:

$$D_c = \frac{1}{N} \sum_{n=1}^N \tilde{y}(t_n) \cos(2\pi\omega_j t_n) \quad D_s = \frac{1}{N} \sum_{n=1}^N \tilde{y}(t_n) \sin(2\pi\omega_j t_n) \quad (15)$$

Equation (14) is not the sole constraint to target the sinusoidal wave corresponding to ω_j because it does not constrain the two free amplitude variables, A_c and A_s . Thus, two additional constraints are incorporated, equating the cosine and sine components of the DFT of the original function, $\tilde{y}(t_n)$, evaluated at ω_j , and the DFT of the approximation, $\tilde{y}_j(t_n)$. These scalar constraint equations are deduced to be of the following form:

$$\Delta D_c = \frac{1}{N} \sum_{n=1}^N [A_j \cos(2\pi\omega_j t_n) + B_j \sin(2\pi\omega_j t_n)] \cos(2\pi\omega_j t_n) - D_c = 0 \quad (16)$$

$$\Delta D_s = \frac{1}{N} \sum_{n=1}^N [A_j \cos(2\pi\omega_j t_n) + B_j \sin(2\pi\omega_j t_n)] \sin(2\pi\omega_j t_n) - D_s = 0 \quad (17)$$

If $\Delta D_c = \Delta D_s = 0$, Equations (16) and (17) reflect the fact that the amplitude and phase of the sinusoidal approximation, $\tilde{y}_j(t_n)$, match the amplitude and phase of the contribution to the original function from the frequency ω_j . Since the frequency and amplitude constraints are expressed in terms of the free variables, the constraints from Equations (14), (16), and (17) are assembled to form the three-dimensional constraint vector, $\bar{F}(\bar{X})$. Given the definitions for the elements of the free variable and constraint vectors, the Jacobian matrix, $D\bar{F}$, is computed and an update equation, at each iteration, i , is formulated using Newton's method to equal:

$$\bar{X}^{i+1} = \bar{X}^i - D\bar{F}(\bar{X}^i)^{-1} \bar{F}(\bar{X}^i) \quad (18)$$

The free variable vector is iteratively updated until the constraint vector is equal to zero, to within a user-specified tolerance. When these constraints are satisfied, the sinusoid described by the free variables is present in the original function, $\tilde{y}(t_n)$.

A straightforward process to generate an initial guess for the resulting differential corrections scheme is developed using the fundamental principles of frequency decomposition. After determining the contribution from $\omega_0 = 0$, each of the M dominant frequencies in $\tilde{y}(t_n)$ are computed in order of decreasing amplitude. The initial guess for the set of parameters that describe each sinusoidal wave is constructed using the FFT algorithm. Each local maximum in the Fourier transform computed by the FFT represents an approximate frequency representation of the original function. The nearby free variables that represent the sinusoidal waves present in the original function are then determined using the described differential corrections algorithm.

Frequency Decomposition of Trajectories

To produce the frequency representation for various types of trajectories, this frequency-refinement technique is explored within the context of the CR3BP. First, a trajectory is selected from the desired region in a Poincaré map that has been constructed using a $y = 0$ surface of section at a specified energy level. Once the map crossing that corresponds to a desired trajectory is identified, the initial state is propagated for approximately 9,000 nondimensional time units and sampled every 0.05 time units to generate a discrete set of data points. The discrete function, created from the x -coordinate in each sample, is multiplied by a Hanning window and initially decomposed into its frequency representation using an FFT algorithm. Each trajectory that is examined in this investigation lies in the exterior region; thus, a frequency analysis of the set of x -components corresponding to the state vectors along the path reveals the underlying frequencies. If any fundamental frequencies are identified from the DFT, the initial guesses for the corresponding sinusoidal waves are corrected using the frequency-refinement targeting scheme.

Features in the DFT are employed to characterize and identify natural trajectories.⁴ A sample quasi-periodic orbit is plotted in both configuration space and the frequency domain in Figure 3 over 100 time units. The location of the two primaries are overlaid as red dots, and the arrow indicates the direction of orbital motion. In Figure 3(b), the DFT constructed from the corresponding orbital data appears, scaled by the maximum amplitude of the computed Fourier coefficients. Multiple peaks are apparent in this frequency representation, each located at linear combinations of the two fundamental frequencies. Exploiting knowledge of the eigenvalues associated with the stable periodic orbit at the center of this quasi-periodic orbit, the largest peak approximately occurs at the frequency denoted ω_1 . The two smaller peaks are located equidistant

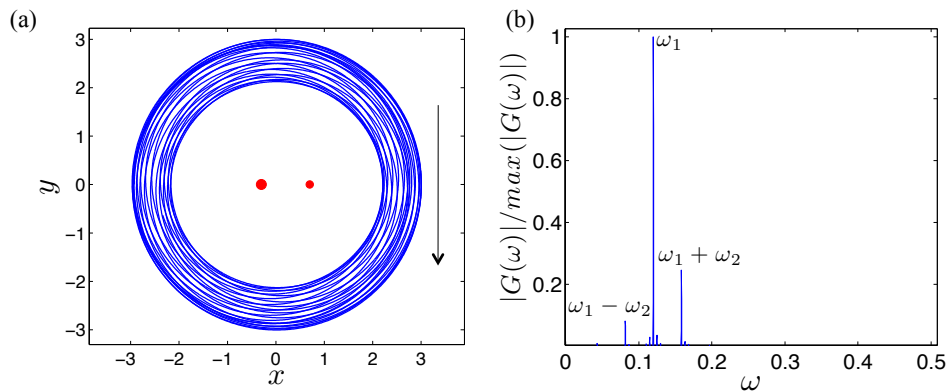


Figure 3. Representation of a quasi-periodic orbit in the (a) configuration space of the CR3BP and (b) frequency domain.

from this dominant peak; this distance is labeled ω_2 . An irrational ratio of these dominant frequencies indicates that the trajectory corresponds to a quasi-periodic orbit. As the contribution from the transverse mode approaches zero, the quasi-periodic orbits in a stable island reduce, in the limit, to the stable periodic orbit at their center. Although a periodic orbit possesses a single fundamental frequency, it can be characterized by the features in its DFT. In fact, for a period- q orbit, stable or unstable, the numerically-detected ratio ω_2/ω_1 is equal to an integer ratio $1/q$ since two independent frequencies do not exist. The ratio of the two dominant frequencies that are present in the DFT of a natural trajectory is, therefore, used to identify the form of the corresponding nonchaotic orbit.

CIRCULAR RESTRICTED THREE-BODY PROBLEM: LARGE MASS RATIOS

Characteristics at $\mu = 0.3$

The process of decomposing a single trajectory into its fundamental frequencies is extended to the frequency representation of the dynamical structures in the CR3BP at a single energy level. Frequency decomposition is applied to the analysis of retrograde trajectories in the vicinity of a stable period-1 orbit located in the exterior region in the CR3BP at a mass ratio $\mu = 0.3$. At discrete values of the energy constant, nearby quasi-periodic orbits are sampled and decomposed into their fundamental frequencies. For each value of the energy constant, the frequency ratio that corresponds to ordered motion intersecting $y = \dot{x} = 0$, forms a one-parameter curve. As an example, consider an energy constant that is equal to the value $C = 3.880149584125780$. The corresponding Poincaré map at $y = 0$, localized to the exterior region, is plotted in Figure 4. The structures captured by this map are located to the left of the two primaries and far beyond the location of L_3 . By observation, the periodic and quasi-periodic orbits form concentric curves and island chains that cross the $\dot{x} = 0$ line, overlaid in blue in the figure. The structures within this region are, therefore, sufficiently represented by considering only trajectories corresponding to map crossings coinciding with the $\dot{x} = 0$ line. For each orbit, a variable x_0 is assigned to represent the nonunique x -coordinate of the map crossing coinciding with the $\dot{x} = 0$ line. In addition, the quantity ω_2/ω_1 is the frequency ratio of the corresponding orbit, computed using the frequency-refinement technique. At the specified energy level, each of the intersecting nonchaotic orbits is, therefore, identifiable using the coordinate pair $(x_0, \omega_2/\omega_1)$.

At a given energy level, the one-parameter curve representing the frequency ratios of quasi-periodic orbits as a function of x_0 reveals the structures visible in a Poincaré map. The frequency ratios, computed for orbits in the vicinity of the stable period-1 orbit at $C = 3.880149584125780$, are plotted in blue in Figure 5. This plot also features red dashed lines at selected, labeled integer ratios. Consider the two intersections of the frequency ratio curve with the $\omega_2/\omega_1 = 1/5$ line: both occur at the same x -coordinate as the intersections of the period-5 island chain with the $\dot{x} = 0$ line on the map depicted in Figure 4. The left-most intersection of the period-5 island chain with the $\dot{x} = 0$ line occurs at an unstable periodic orbit; on the right, a stable

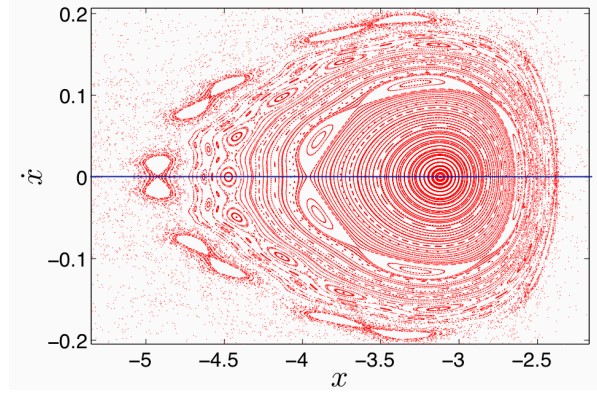


Figure 4. Poincaré map at $C = 3.880149584125780$ for $\mu = 0.3$, constructed using a $y = 0$ section, localized to the exterior region in the CR3BP.

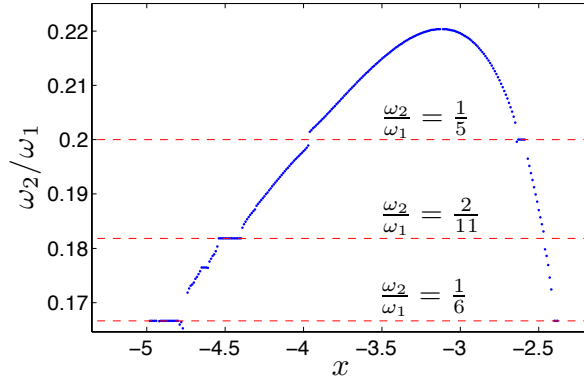


Figure 5. Frequency representation of retrograde periodic and quasi-periodic orbits in the vicinity of the stable period-1 orbit in the exterior region for $\mu = 0.3$ at an energy level $C = 3.880149584125780$.

period-5 orbit intersects the $\dot{x} = 0$ line. Correspondingly, these two intersections appear distinctly different in the frequency representation: the unstable orbit appears as a steep change in the frequency ratio, while the frequency ratio at the location of the stable orbit lies at the center of a plateau formed by the numerically-detected frequency ratios of its surrounding quasi-periodic orbits. Extending these observations, any stable or unstable period- q orbit is identified and located on the frequency ratio curve when the previously described features are centered about the integer ratio, p/q for $q > 1$ and $p < q$. As demonstrated in this example, the denominator of the corresponding ratio equals the q map crossings of a retrograde period- q orbit in the exterior region. In addition, the sum $p + q$ is approximately equal to the ratio of the orbital period to the period of the primaries; this property is apparent using any differentially corrected period- q orbit. Thus, the one parameter frequency ratio curve reveals the presence of quasi-periodic orbits and some qualitative properties of any embedded period- q orbits.

A frequency representation of the structures present over a range of energy levels introduces a third parameter identifying each orbit: its energy level. A single orbit is, therefore, described by the tuple $(x_0, \omega_2/\omega_1, C)$. Accordingly, ordered motion within a specified range of energy levels forms a two-parameter surface when represented using frequency ratios. To reduce the complexity in visualizing the resulting surface approximation, simple two-dimensional representations of this three-dimensional information are constructed. Due to the inherent loss of information, the specific configuration must be tailored to the immediate goal.

To represent the form and stability of ordered motion, the frequency ratio is plotted for each value of x_0 that identifies an orbit at any energy level. An example of this concept is depicted in Figure 6 for retrograde

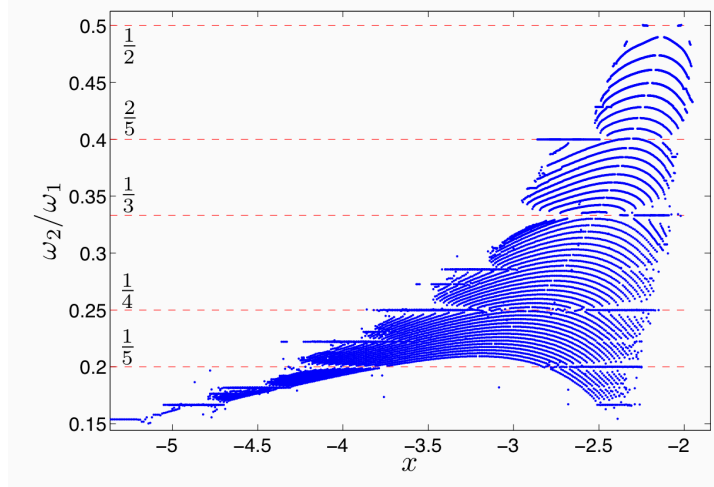


Figure 6. Composite representation of the frequency ratios of retrograde periodic and quasi-periodic orbits in the exterior region in the CR3BP with $\mu = 0.3$ for energy levels between $C(L_1)$ and $C(L_3)$.

periodic and quasi-periodic orbits in the exterior region in the CR3BP at a mass ratio of $\mu = 0.3$ for energy levels between $C(L_1)$ and $C(L_3)$. Overlaid on this plot are red dashed lines indicating the integer ratios corresponding to selected low-order period- q orbits. Analysis of this figure reveals that the frequency ratio passes through integer ratios, m/q , reflecting various period- q orbits, signaling the existence of the corresponding orbits within the specified energy range. Consider the curves intersecting the integer ratio $\omega_2/\omega_1 = 1/3$. The lack of data points on the left half of this intersection reveals the location of the unstable orbit within a period-3 chain, while the horizontal accumulation of points on the right side indicates the stable period-3 orbit and its surrounding quasi-periodic motion. Features in the frequency domain representation, therefore, represent, qualitatively, the stability of nonchaotic motion over a range of energy levels.

To determine the boundaries of a structure within the phase space and the energy levels at which it exists, a two-dimensional representation is constructed using approximate level sets of the frequency ratio. Given a period- q orbit that possesses the frequency ratio p/q , its corresponding level set at the frequency ratio is approximated by processing the discretely sampled tuples $(x_0, \omega_2/\omega_1, C)$. If the period- q orbit is stable, its associated quasi-periodic orbits are represented by plotting the (x_0, C) coordinates of orbits with frequency ratios in the range $(p/q - \epsilon) < \omega_2/\omega_1 < (p/q + \epsilon)$, for a reasonably small, positively-valued ϵ . Only the periodic orbit has a frequency ratio exactly equal to p/q ; however, its surrounding quasi-periodic orbits possess frequency ratios close to the integer ratio. An example of the constructed representation is plotted in Figure 7 for selected retrograde period- q orbits, and their surrounding quasi-periodic motion, located in the exterior region in the CR3BP at a mass ratio of $\mu = 0.3$; the corresponding families are labeled as “P- q ”. On the vertical axis, the energy constant computed for each orbit is scaled using the difference $C(L_2) - C(L_3)$. The energy levels corresponding to L_2 and L_3 are used as a reference because these two Lagrange points bound motion between the interior and exterior regions. To represent the unstable periodic orbits present in a period- q chain, the energy and appropriate x -crossing of the unstable orbit are obtained using continuation. This composite frequency representation in Figure 7 depicts the extent of the periodic orbits in a period- q island chain within the phase space, for various values of the energy. The regions about each curve, representing a family of periodic orbits, are populated by quasi-periodic orbits; the spread of points from the curve describing the periodic orbits represents the extent of ordered motion that persists within the phase space.

Together, the two composite frequency representations in Figures 6 and 7 offer information about ordered motion in the exterior region in the CR3BP at energy constants between $C(L_1)$ and $C(L_3)$. As plotted in Figure 6, each frequency ratio curve, computed at a single energy level, features an undefined maximum

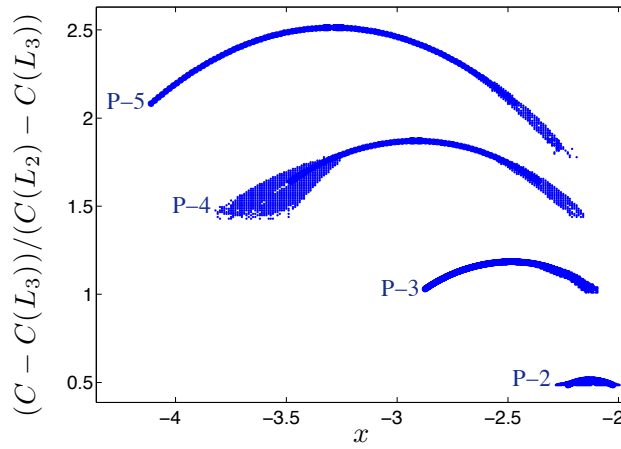


Figure 7. Composite representation of the energy levels of selected retrograde period- q orbits and their surrounding quasi-periodic orbits. These orbits are located in the exterior region in the CR3BP.

frequency ratio corresponding to the period-1 orbit at the center of the stable island. The frequency ratio is undefined at this location because periodic orbits are only described by one frequency. A quasi-periodic orbit that exists farther from the central period-1 orbit exhibits a lower frequency ratio. Furthermore, decreasing the energy constant results in each curve encompassing higher frequency ratios, and over the range of energy constants that are examined, a variety of low-order period- q orbits exist. Recall Figure 7, which features a selection of these orbits with the frequency ratio $1/q$; each orbit family is formed at an energy constant equal to the highest energy constant of the period- q family in this frequency representation. The stable orbits in the resulting island chain are surrounded by quasi-periodic orbits, which extend farther into the phase space with decreasing energy constant, until reaching a critical value of the energy constant. Then, the stable islands rapidly decrease in size as the period- q orbits approach a fold bifurcation. Combining the two frequency representations, therefore, allows for the description and characterization of the range of dynamics present in the exterior region in the CR3BP at a mass ratio of 0.3.

Influence of the Mass Ratio: $0.2 \leq \mu \leq 0.4$

Additional insight into the CR3BP is gained through a frequency analysis of the stable structures present at various large values of the mass ratio, within the range $\mu = [0.2, 0.4]$. A frequency analysis is completed for orbits in the exterior region in the CR3BP for the sample mass ratios $\mu = 0.2$, $\mu = 0.3$, $\mu = 0.4$, which lie in the range of large mass ratios typical of many known binary star systems. The resulting composite frequency representation is displayed in Figure 8. The impact of the mass ratio on two specific characteristics of period- q families of orbits may be discerned from this frequency representation. First, the range of frequency ratios encompassed by ordered motion in the exterior region decreases with decreasing mass ratio, and vice versa. Correspondingly, a smaller range of period- q orbits are available for lower mass ratios within the specified bounds. Consider, for example, a period-5 orbit with frequency ratio $1/5$. Since the range of frequency ratios encompassed by the mass ratios $\mu = 0.3$ and $\mu = 0.4$ includes the frequency ratio $1/5$, a period-5 island chain is present within the energy interval $C = [C(L_1), C(L_3)]$. At a mass ratio of $\mu = 0.2$, however, the selected period-5 island chain is only accessible over a small interval of energy constants within this range, far from the energy constant at which the period-multiplying bifurcation occurs to form this family of orbits. To further ascertain the effect of this dependence of the frequency ratio range on the mass ratio, the energy of each quasi-periodic orbit is plotted as a function of its frequency ratio in Figure 9. Analysis of this figure suggests that higher order period- q orbits with a low frequency ratio are available at higher values of the energy constant for a mass ratio of $\mu = 0.4$ than at a mass ratio of $\mu = 0.3$. However, this observation is not applicable to larger frequency ratios. As an example, consider a mass ratio of $\mu = 0.4$. At this value of the mass ratio, a period-2 orbit is accessible at a energy constant, relative to that of L_2 and L_3 , that is lower

than at a mass ratio of $\mu = 0.3$. In addition, the stable orbits in the exterior region do not seem to encompass a significantly different region of the phase space over the specified range of mass ratios; this observation is deduced from Figure 8. Similar analyses may also be accomplished in the MCR3BP for various values of the three-body potential coefficient, k ; a comparison of the results to the analysis performed in this section aids in understanding any effects of the three-body interaction that may not be reproducible by changing the natural parameters in the CR3BP, including the energy constant and the mass ratio.

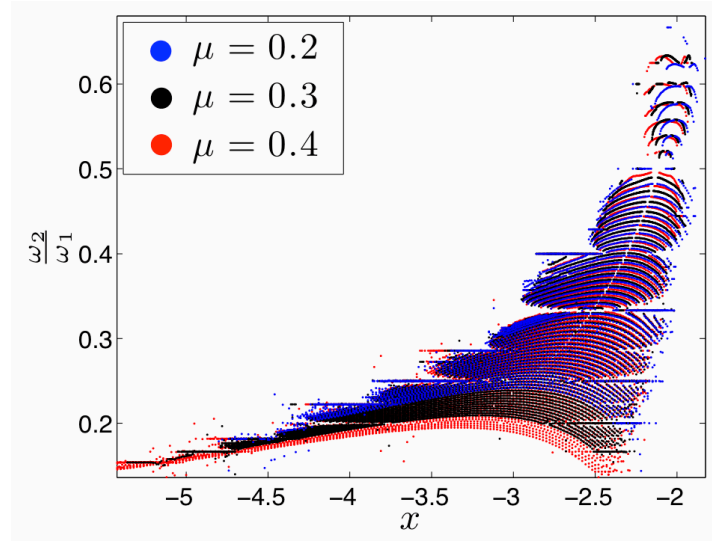


Figure 8. Composite representation of the frequency ratios of retrograde periodic and quasi-periodic orbits in the exterior region in the CR3BP for energy levels between $C(L_1)$ and $C(L_3)$ at mass ratios equal to 0.2 (blue), 0.3 (black), and 0.4 (red).

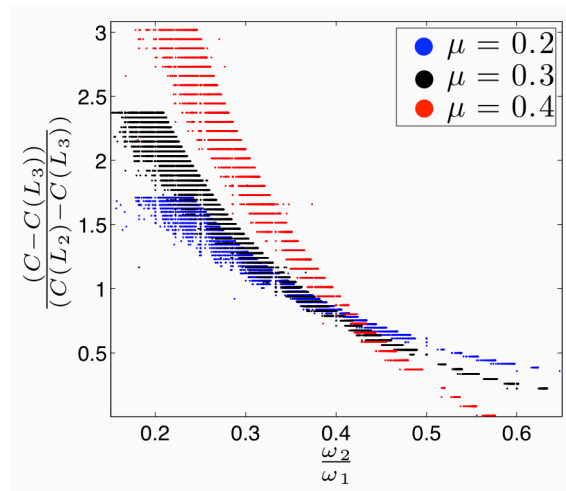


Figure 9. Representation of the frequency ratios and energy levels of retrograde periodic and quasi-periodic orbits in the exterior region in the CR3BP at mass ratios equal to 0.2 (blue), 0.3 (black), and 0.4 (red).

CHARACTERISTICS OF THE THREE-BODY INTERACTION

By combining techniques developed in dynamical systems theory and frequency analysis, a subset of the underlying dynamical structures in the MCR3BP are examined over a range of values of the three-body potential coefficient, limited to $k = [-0.2, 0.8]$. During the following analysis, the mass ratio in the MCR3BP is held constant at $\mu = 0.3$.

Equilibrium Points

The existence and location of the equilibrium points offer preliminary insight into the impact of a three-body interaction, for various values of the coefficient k , on the dynamical environment in the MCR3BP. Solving the equations of motion when the accelerations and velocities are set equal to zero, the equilibrium points in the MCR3BP are located for various values of k .⁴ The five equilibrium points that exist in the range $k = [-0.2, 0.8]$ are plotted in Figure 10. In this figure, the green dots indicate the location of the five equilibrium points in the CR3BP for a mass ratio $\mu = 0.3$. The equilibrium points for positive values of k in the specified interval appear as blue dots in the figure, while red dots locate the equilibrium points corresponding to negative values of k . Since the MCR3BP is formulated to reduce to the CR3BP as the coefficient k approaches zero, equilibrium points computed for increasing magnitudes of the three-body potential coefficient exist farther from the equilibrium points in the CR3BP. As an example, the location of L_4 is labeled in Figure 10 for $k = -0.2, 0.0, 0.8$. Analysis of this figure reveals that, for increasingly positive values of the three-body potential coefficient, the collinear equilibrium points are located farther from P_2 . The location of L_1 varies less for positive values of k than the locations of L_2 and L_3 since L_1 exists between the two primaries, where the inverse-square gravitational forces act in opposing directions. Furthermore, in the MCR3BP, the triangular equilibrium points, L_4 and L_5 , are no longer located at the vertices of an equilateral triangle as in the CR3BP; instead, they exist farther from the primaries. For negative values of k , the equilibrium points are all located closer to P_2 than the equilibrium points in the CR3BP. In addition, the locations of the triangular equilibrium points appear most sensitive to negative values of k , when the three-body interaction opposes the gravitational forces.

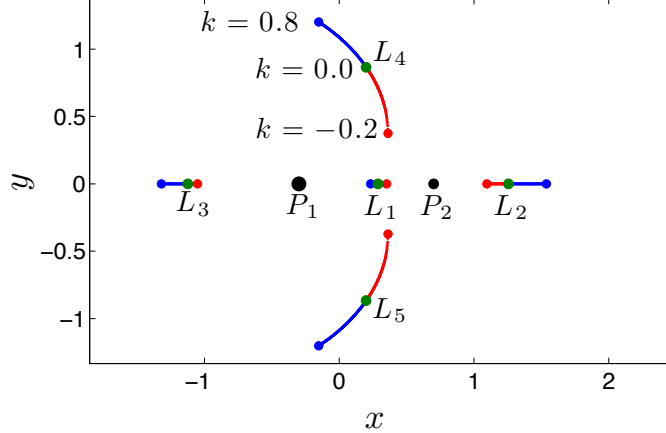


Figure 10. Location of equilibrium points for values of the three-body potential coefficient in the range $k = [-0.2, 0.8]$.

Another effect of the three-body interaction emerges when the energy constant is evaluated at each equilibrium point for various values of the constant, k , that scales the additional term. These energy constants, $C(L_i)$, are plotted in Figure 11 and colored as indicated in the legend. Note that, due to symmetry, the value of the energy constant at the triangular equilibrium points are equivalent. For increasingly positive values of k within the specified range, the energy constant evaluated at each equilibrium point increases. For increasingly negative values of k , however, the values of the energy constants $C(L_i)$ in the MCR3BP do not maintain an

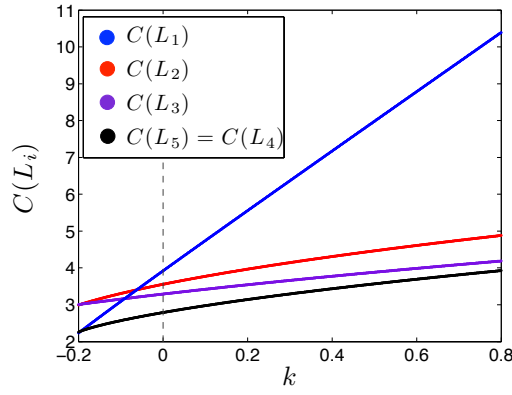


Figure 11. Energy constant evaluated at the equilibrium points for the range $k = [-0.2, 0.8]$.

order, by magnitude, that is consistent with the order of the $C(L_i)$ values in the CR3BP. Physically, this change in the order of the values of the energy constants $C(L_i)$ translates to the L_i gateways opening in a different order for a decreasing energy constant, or, equivalently, increasing energy. For example, consider the MCR3BP when $k = -0.1$: comparison of the energy constant at the three collinear equilibrium points reveals that the L_2 gateway will open at the lowest energy, or the highest value of the energy constant. Although P_3 can travel between the exterior and P_2 regions, it cannot cross into the P_1 region. Within the context of the CR3BP, this scenario is not possible, indicating that a three-body interaction opposing the two inverse-square gravitational forces can modify the regions that can be traversed along a single, natural trajectory.

Zero Velocity Curves

The regions of allowable motion in the MCR3BP, for various values of k , are straightforwardly visualized using zero-velocity curves, commonly employed in analysis of the CR3BP.⁴ For a specified value of the three-body coefficient, the shape and location of the ZVCs depend upon the energy constant; however, insight into the possible motion in the planar MCR3BP is obtained by analyzing the ZVCs at the values of the energy constant corresponding to the three collinear equilibrium points. The ZVCs at these three distinct energy levels are plotted in Figure 12 for the following values of the three-body coefficient: (a) $k = 0.0$, (b) $k = -0.1$, and (c) $k = 0.4$. To aid in visual clarity, the ZVCs at $C(L_1)$, $C(L_2)$, and $C(L_3)$ are colored blue, red, and green, respectively. Additionally, the equilibrium points are represented as black diamonds and the primaries are indicated by black filled circles.

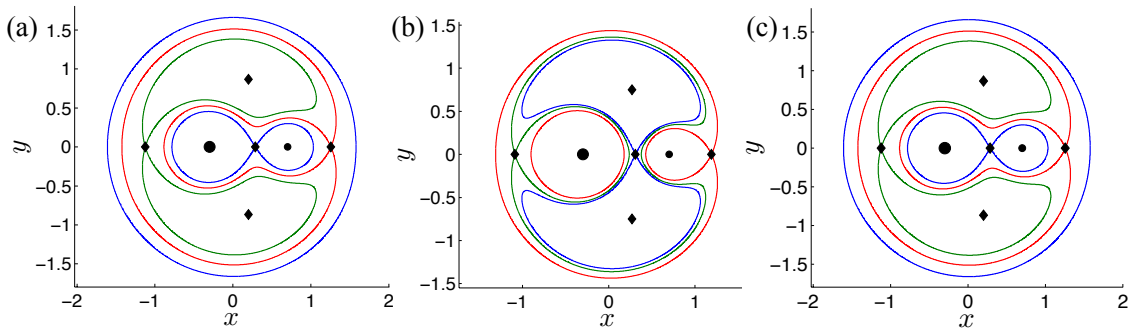


Figure 12. Zero velocity curves at the values of $C(L_1)$ (blue), $C(L_2)$ (red), and $C(L_3)$ (green) corresponding to the three collinear equilibrium points for (a) $k = 0$, (b) $k = -0.1$, and (c) $k = 0.4$ in the MCR3BP.

The ZVCs plotted for $k = -0.1$ reveal that for an energy constant equal to $C(L_1)$, P_3 can travel through the L_2 and L_3 gateways, allowing motion between the vicinity of a primary and the exterior region. However, a natural trajectory cannot move directly between P_1 and P_2 without traversing the exterior region; such a dynamical constraint is not known to exist in the planar CR3BP at any value of the mass ratio. This shape for the ZVC boundaries corresponds to $C(L_1)$ possessing a lower value than the energy constants $C(L_2)$ and $C(L_3)$. For the ZVCs plotted at these two larger values of the energy constant, the forbidden regions encompass less of the exterior region than the ZVCs at a comparable energy level in the CR3BP.

For a positive three-body potential coefficient, $k = 0.4$, the ZVCs loosely resemble those in the CR3BP, with some small differences. One example is that the ZVCs at $C(L_1)$, evaluated in the MCR3BP, extend farther into the interior and exterior regions. However, decreasing the energy constant reveals that more of the interior region is accessible to P_3 at higher energies. Consequently, at an energy constant equal to $C(L_2)$, the increased size of the L_1 gateway results in a larger range of trajectories passing between the vicinities of both primaries than in the CR3BP. This increase in the size of the L_1 gateway may impact the properties and the types of periodic solutions that are available within the interior region in the MCR3BP.

Periodic and Quasi-Periodic Structures in the Exterior Region

The previous composite frequency representations are employed to compare periodic and quasi-periodic orbits in the MCR3BP, with the mass ratio fixed at $\mu = 0.3$. Given that a three-body interaction may be attractive or repulsive, the MCR3BP is analyzed for selected positive and negative values of the three-body potential coefficient. In particular, this investigation focuses on three properties of the dynamical characteristics that are observed in the exterior region: the form of stable structures, the energy levels at which these structures are available, and their extent within the phase space.

For positive three-body potential coefficients below a critical value, period- q orbits that are present in the CR3BP also exist in the MCR3BP. In Figure 13, the frequency ratios corresponding to orbits within the central stable island are plotted for various energy levels in the range $C = [C(L_3), C(L_1)]$ in the CR3BP (blue) and in the MCR3BP for $k = 0.1$ (green). Analyzing this figure, the frequency ratios of the orbits that exist when $k = 0.1$ encompass a larger range of integer ratios than in the CR3BP for a mass ratio $\mu = 0.3$. Thus, periodic orbits existing within this specific range of energy constants in the CR3BP are also present over a comparable range of energy levels in the MCR3BP for $k = 0.1$. This effect is similar to increasing the mass ratio, but cannot be reproduced using a reasonable value for μ . The low-order period- q orbits in the MCR3BP, over the range of positive coefficients examined in this investigation, appear qualitatively similar to the CR3BP when represented in the frequency domain. Since they appear consistent between the MCR3BP for $k = 0.1$ and the CR3BP, the frequency analysis process reveals a similar configuration for the stable and unstable orbits within the visible period- q island chains. The phase space representations of stable, low-order period- q orbits do not exhibit any structural differences between the CR3BP and the MCR3BP, for positive values of the three-body coefficient.

For attractive three-body interactions in the MCR3BP, period- q islands appear to exist at lower energy constants than in the CR3BP and extend farther into the phase space. This information is extracted by considering the energy levels and the locations of a selected set of period- q orbits with frequency ratios $1/q$, as plotted in Figure 14 which includes $k = 0.1$ (green) and $k = 0$ (blue). Analysis of this figure reveals that, incorporating an attractive three-body interaction, each of the selected, stable period- q structures is accessible over a smaller range of energy values that are lower in magnitude relative to the difference $C(L_2) - C(L_3)$. Additionally, the bounds on the quasi-periodic motion about resonant orbits, appear to exist farther from the corresponding period- q orbit. These observations are not consistent with the previous analysis, suggesting that this change in the stable motion is not reproducible by changing the mass ratio in the CR3BP.

Beyond a critical positive value of the three-body potential coefficient, period-multiplying bifurcations influence the underlying periodic orbits in the MCR3BP and, therefore, the surrounding quasi-periodic motion. In Figure 14, the level sets corresponding to selected period- q orbits for $k = 0.6$ represent quasi-periodic orbits that exhibit behavior that is not consistent with the CR3BP. Consider, for example, the leftmost island surrounding a stable period-4 orbit in Figure 14. The location of the outermost quasi-periodic orbit in the

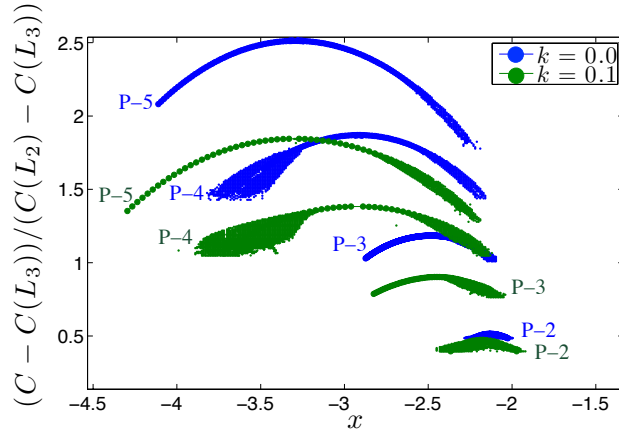


Figure 13. Composite frequency representation of retrograde orbits over various energy levels in the range $C = [C(L_3), C(L_1)]$, for $k = 0.0$ (blue) and $k = 0.1$ (green).

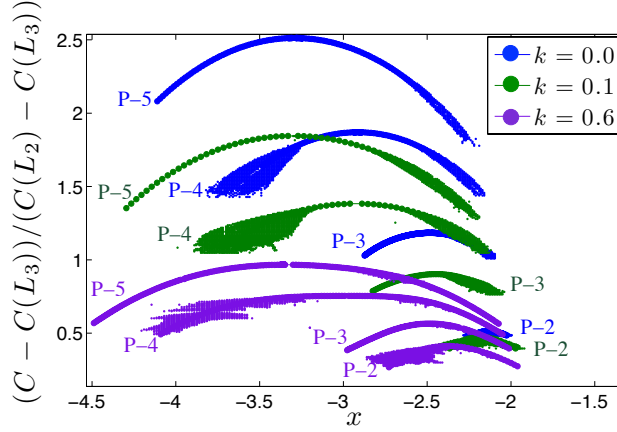


Figure 14. Composite representation of the energy levels of selected retrograde period- q orbits (with frequency ratio $1/q$) and their surrounding quasi-periodic orbits, for $k = 0.0$ (blue), $k = 0.1$ (green) and $k = 0.6$ (magenta).

stable island clearly fluctuates over the range of energy levels where a stable period-4 orbit exists. An explanation for this behavior emerges from a stability analysis of the underlying family of periodic orbits. The stability index, s , for this family of planar orbits is plotted in Figure 15 as a function of the energy value. Overlaid on the stability index curve are two red lines located at the critical stability indices $s = -2$ and $s = +2$, the former corresponding to a period-doubling bifurcation. Additionally, the black lines represent selected, labeled period-multiplying bifurcations. Analyzing this figure, the family of period-4 orbits undergoes successive period-multiplying bifurcations for multiplicative factors greater than 2. Since the stability index does not graze or pass through the value $s = -2$, a period-doubling bifurcation does not occur along this family. The top and bottom insets of Figure 15 depict Poincaré maps constructed at energy levels below those corresponding to period-multiplying bifurcations for the multiplicative factors 5 and 3, respectively. Each map is "zoomed-in" to the vicinity of one of the period-4 stable islands. Considering the top inset, a period-4 orbit family has created a family of period-20 orbits at a nearby energy level. Given that this new family of orbits also has a frequency ratio equal to $1/4$, the period-multiplying bifurcation is not detectable on the frequency representations. Instead, the presence of these bifurcations is reflected in the shape of the level sets in Figure 14. Since this dynamical behavior is not observed in this region in the CR3BP for a mass ratio in the range $\mu = [0.2, 0.4]$, significantly large positive values of the three-body potential coefficient apparently induce period-multiplying bifurcations along families of period- q orbits.

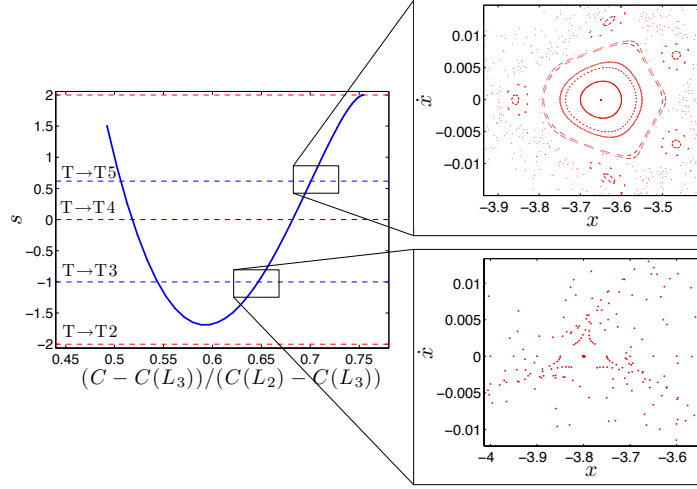


Figure 15. Stability index for selected stable period-4 orbits in the MCR3BP for a three-body potential coefficient $k = 0.6$, with dotted lines at the stability indices corresponding to selected bifurcations. In the insets, zoomed-in views of the Poincaré map near highlighted period-multiplying bifurcations.

The critical positive value of k at which certain period-multiplying bifurcations occur depends upon the family of period- q orbits. This observation is straightforwardly supported by an analysis of the stability index of various orbit families at a single value of the three-body coefficient. As an example, consider the stability index over some interval of the period-2 to period-5 orbit families plotted in Figure 16 for $k = 0.6$. The frequency ratio along these families is equal to $\omega_2/\omega_1 = 1/q$. In comparison to the CR3BP for mass ratios in the range $\mu = [0.2, 0.4]$, the stability indices of the plotted intervals of the period- q families pass through a wider range of values of s , with the minimum values along these curves varying between each family. The period-5 family passes through $s = -2$, undergoing a period-doubling bifurcation at two values of the energy constant. Between these bifurcations, the members of the family are unstable. This bifurcation does not occur along this period-5 orbit family in the CR3BP for a large mass ratio within the range of mass ratios that has been examined. Since the minimum along the curve reflecting the stability index for part of the period-3 family does not pass through $s = -2$ or $s = -1$ for a three-body potential coefficient of $k = 0.6$, the period-3 family does not undergo period-tripling or period-doubling bifurcations. Extending this analysis to periodic orbits in the MCR3BP for different values of k reveals that these bifurcations do occur in the period-3 family for larger values of the three-body coefficient. Thus, the value of the positive coefficient k for which period-multiplying bifurcations are present along families of period- q orbits, where $q > 1$, depends upon the family.

Negative three-body potential coefficients, smaller in magnitude than a critical value, influence the dynamics in the MCR3BP by reducing the size of the regions of stable motion and the energy levels at which they exist. The composite frequency representation in Figure 17 depicts the level sets of selected period- q orbits and their associated quasi-periodic motion for $k = 0.0$ (blue), $k = -0.01$ (black) and $k = -0.1$ (grey). The stable period- q orbits, for negative values of k , are available at higher energy constants, and over a smaller range. In addition, the regions of stable motion surrounding the selected families of periodic orbits contract in the x -direction for $k = -0.01$. This observation is clear from the level sets in Figure 17, which do not deviate as far from the period- q orbits as those in the CR3BP for a mass ratio of $\mu = 0.3$.

For a larger negative value of the three-body potential coefficient, the dynamical structures in the exterior region do not resemble those in the CR3BP over the range of mass ratios that has been examined. In fact, the frequency analysis process employed in this investigation only captures stable islands for period- q island chains with an odd value of q . In contrast to the CR3BP, each of these families exhibits a change in the

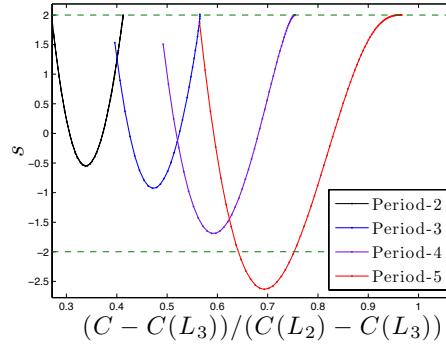


Figure 16. Stability index curves for period-2 to period-5 orbits in the MCR3BP for $k = 0.1$.

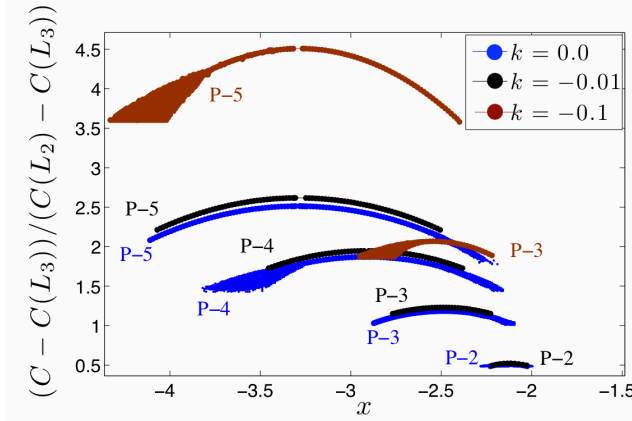


Figure 17. Composite representation of the energy levels of selected retrograde period- q orbits (with frequency ratio $1/q$) and their surrounding quasi-periodic orbits, for $k = 0.0$ (blue), $k = -0.01$ (black) and $k = -0.1$ (grey).

location of the stable and unstable period- q orbits within the corresponding island chain. This observation is illustrated by the period-5 island chains in the Poincaré maps plotted in Figure 18 for (a) the CR3BP with $\mu = 0.3$ and (b) the MCR3BP with $k = -0.1$. For even values of q , however, the change in the stability of the orbits in a period- q island chain results in the frequency analysis process detecting only unstable orbits. To analyze the stable orbits within the island chain, an alternative approach for representing the frequency decomposition of orbits within an island is appropriate for further investigation of the influence of a three-body potential term.

CONCLUSION

Augmenting the pairwise gravitational potential in the CR3BP with a three-body interaction, scaled by the coefficient k , impacts the stable solutions available to a particle orbiting in the exterior region. The influence of this additional term on the dynamical structures in the MCR3BP, for a mass ratio of $\mu = 0.3$, is explored using both dynamical systems theory and frequency analysis. Investigation of particular solutions in the form of equilibrium points and zero velocity curves reveals a change in the bounds on the motion of P_3 . Modeling the MCR3BP with a positive three-body coefficient, k , the size of the regions of allowable motion differs from the bounded regions in the CR3BP. For a large negative coefficient, however, the zero velocity curves can exhibit significantly different features since the L_i gateways open in a different order for $i = 1, 2, 3$. This change in the shape of the zero velocity curves may impact the orbits available in the MCR3BP.

Frequency decomposition is employed to locate and represent the periodic and quasi-periodic orbits that form the underlying structure of the dynamical environment in the augmented model. Within the range of

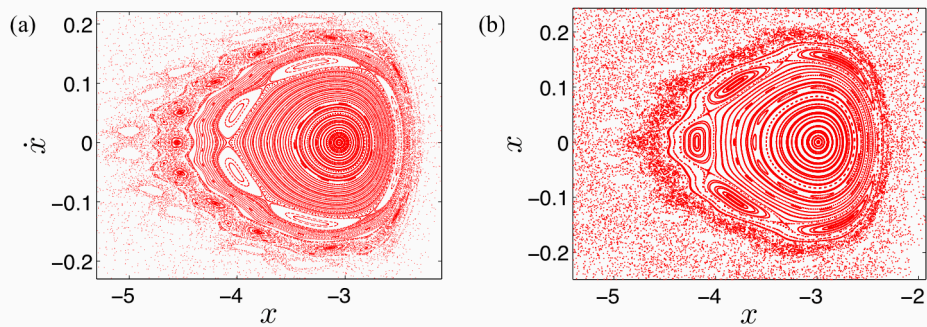


Figure 18. Poincaré maps depicting period-5 island chains in the MCR3BP for (a) $k = 0.0$ and (b) $k = -0.1$.

three-body coefficients considered in this investigation, the period- q orbits present in the CR3BP are also available in the MCR3BP. The value of the three-body coefficient affects the energy levels at which these orbit families are accessible. In addition, the three-body interaction affects the size of the stable regions within the phase space. For sufficiently large values of k , period-multiplying bifurcations occur along families of period- q orbits, as apparent in the frequency representations and confirmed using Poincaré maps. Selecting a large negative value of k , however, impacts the location of stable and unstable orbits within a period- q island chain, suggesting a change in the formation of the two period- q orbit families. These changes in the dynamical environment suggest that the three-body interaction influences the underlying structure of the MCR3BP with an effect that may not be reproducible by modifying the energy constant or the large mass ratio in the CR3BP.

ACKNOWLEDGEMENTS

The authors wish to express their gratitude towards the School of Aeronautics and Astronautics at Purdue University, the Purdue University Lynn Fellowship, and the Purdue Graduate Student Government Travel Fund for their financial support of this research and attendance at this conference. The authors also wish to thank Ingrid Stairs for her helpful communications.

REFERENCES

- [1] M. H. van Kerkwijk, C. G. Bassa, B. A. Jacoby, P. G. Jonker, "Optical Studies of Companions to Millisecond Pulsars," *Astronomical Society of the Pacific Conference Series*, Vol. 328, pp. 357-369, 2005.
- [2] E. Fischbach, "Long-Range Forces and Neutrino Mass," *Annals of Physics*, vol. 247, pp. 213-291, 1996.
- [3] E. B. Ford, K. J. Joshi, F. A. Rasio, B. Zbarsky, "Theoretical Implications of the PSR B1620-26 Triple System and its Planet," *Astrophysical Journal*, Vol. 528, pp. 336-350, 2000.
- [4] N. Bosanac, "Exploring the Influence of a Three-Body Interaction Added to the Gravitational Potential Function in the Circular Restricted Three-Body Problem: A Numerical Frequency Analysis," M.S Thesis, School of Aeronautics and Astronautics, Purdue University, West Lafayette, Indiana, December 2012.
- [5] V. Szebeheley, *Theory of Orbits: The Restricted Problem of Three Bodies*. London, UK: Academic Press, 1967.
- [6] T.S. Parker, L.O Chua, *Practical Numerical Algorithms for Chaotic Systems*. New York: Springer-Verlag, 1989.
- [7] G. Contopoulos, *Order and Chaos in Dynamical Astronomy*. Germany: Springer-Verlag, 2002.
- [8] W. S. Koon, M. W. Lo, J. E. Marsden, S. D. Ross, *Dynamical Systems, the Three Body Problem and Space Mission Design*, 2006.
- [9] L. Perko, *Differential Equations and Dynamical Systems*. Third Edition, New York: Springer, 2000.
- [10] R. Seydel, *Practical Bifurcation and Stability Analysis: From Equilibrium to Chaos*. New York: Springer-Verlag, 1994.
- [11] J. Laskar, "Frequency Map Analysis of an Hamiltonian System," *American Institute of Physics Conference Proceedings*, 1995.